PNAS RESEARCH ARTICLE | BIOCHEMISTRY CHEMISTRY

Amino acid and protein specificity of protein fatty acylation in *C. elegans*

Bingsen Zhang[a,b], Yan Yu[a,b], Bennett W. Fox[a,b], Yinong Liu[b], Venkatesh P. Thirumalaikumar[a], Aleksandra Skirycz[a], Hening Lin[b,c,d], and Frank C. Schroeder[a,b,1]

Edited by Bryan Dickinson, University of Chicago Division of the Biological Sciences, Chicago, IL; received May 8, 2023; accepted December 21, 2023 by Editorial Board Member Susan Strome

Protein lipidation plays critical roles in regulating protein function and localization. However, the chemical diversity and specificity of fatty acyl group utilization have not been investigated using untargeted approaches, and it is unclear to what extent structures and biosynthetic origins of *S*-acyl moieties differ from *N*- and *O*-fatty acylation. Here, we show that fatty acylation patterns in *Caenorhabditis elegans* differ markedly between different amino acid residues. Hydroxylamine capture revealed predominant cysteine *S*-acylation with 15-methylhexadecanoic acid (isoC17:0), a monomethyl branched-chain fatty acid (mmBCFA) derived from endogenous leucine catabolism. In contrast, enzymatic protein hydrolysis showed that N-terminal glycine was acylated almost exclusively with straight-chain myristic acid, whereas lysine was acylated preferentially with two different mmBCFAs and serine was acylated promiscuously with a broad range of fatty acids, including eicosapentaenoic acid. Global profiling of fatty acylated proteins using a set of click chemistry–capable alkyne probes for branched- and straight-chain fatty acids uncovered 1,013 *S*-acylated proteins and 510 hydroxylamine-resistant *N*- or *O*-acylated proteins. Subsets of *S*-acylated proteins were labeled almost exclusively by either a branched-chain or a straight-chain probe, demonstrating acylation specificity at the protein level. Acylation specificity was confirmed for selected examples, including the *S*-acyltransferase DHHC-10. Last, homology searches for the identified acylated proteins revealed a high degree of conservation of acylation site patterns across metazoa. Our results show that protein fatty acylation patterns integrate distinct branches of lipid metabolism in a residue- and protein-specific manner, providing a basis for mechanistic studies at both the amino acid and protein levels.

protein lipidation | click chemistry | proteomics | branched-chain fatty acids | *C. elegans*

Significance

Fatty acylation is essential for anchoring many proteins to cell and organelle membranes where they exert their functions. Protein function can further depend on the specific identity of the fatty acyl moiety; however, protein fatty acylation patterns in many model organisms have not been comprehensively investigated. Using untargeted approaches, we show that in *Caenorhabditis elegans*, cysteine, glycine (N-terminal), lysine, and serine exhibit unexpectedly diverse fatty acylation profiles, whereby different amino acids are acylated with fatty acids from different biosynthetic pathways. Global profiling of fatty acylated proteins via click chemistry further revealed acylation specificity at the individual protein level. Our findings show how protein function is broadly coupled to distinct branches of lipid metabolism and provides a basis for mechanistic studies.

Protein fatty acylation, along with other types of protein lipidation (e.g., cysteine prenylation), dramatically alters protein hydrophobicity and behavior, regulating trafficking, localization, as well as protein–protein and protein–membrane interactions (1–4). Correspondingly, changes in protein fatty acylation have been implicated in a wide range of human diseases, including cancer (5, 6), neurodegeneration (7), vascular disorders (8), as well as bacterial (9) and viral infection (10, 11). Building evidence for the incorporation of diverse fatty acyl moieties at different sites hints at complex inter- and intra-cellular signaling networks (12–14); however, it remains unclear to what extent the identities and biosynthetic origins of fatty acyl moieties attached to different amino acids vary.

Proteins can be fatty acylated via thioester (*S*-linked, via cysteine), amide (*N*-linked, via protein N-terminal glycine and lysine sidechain), and ester (*O*-linked, via serine and, occasionally, threonine) (1). Whereas it is well established that N-terminal glycine is predominantly acylated with myristoyl (C14:0) (15), differences between the profiles of *S*-, *O*-, and lysine *N*-acylation have not been comprehensively investigated. Palmitoyl (C16:0) is generally presumed to be the predominant *S*-linked cysteine modification, although some studies suggest that *S*-acyl profiles vary among different cell lines (16) and are affected by dietary fatty acids (17). Knowledge of serine and lysine fatty acylation is comparatively limited, and the diversity of fatty acyl moieties attached to these two residues has not been investigated at the proteome level (18, 19).

The nematode *Caenorhabditis elegans* is a highly tractable model system for developmental biology and neuroscience, and, correspondingly, protein trafficking (20) and lipid metabolism (21) in *C. elegans* have been extensively investigated. The *C. elegans* genome encodes putative orthologs of conserved *dhhc S*-acyltransferases as well as orthologs of human acyl-protein thioesterases, *ath-1*, *aho-3*, and *ppt-1* (22). Although reversible cysteine fatty acylation plays an indispensable role in many regulatory events, little is known about

Author contributions: B.Z. and F.C.S. designed research; B.Z., Y.Y., B.W.F., Y.L., and V.P.T. performed research; B.Z. and H.L. contributed new reagents/analytic tools; B.Z., B.W.F., Y.L., V.P.T., A.S., and F.C.S. analyzed data; and B.Z. and F.C.S. wrote the paper.

Competing interest statement: H.L. is a founder of, consultant, and a stockholder for Sedec Therapeutics. F.C.S. is a founder of, consultant, and a stockholder for Ascribe Bioscience and Holoclara Inc.

This article is a PNAS Direct Submission. B.D. is a guest editor invited by the Editorial Board.

[1]To whom correspondence may be addressed. Email: fs31@cornell.edu.

This article contains supporting information online at https://www.pnas.org/lookup/suppl/doi:10.1073/pnas.2307515121/-/DCSupplemental.

Published January 22, 2024.

S-acylation in *C. elegans*, reflecting a general lack of characterization of *C. elegans* fatty acylated proteins in this important model organism.

In this work, we employed two complementary high-resolution mass spectrometry (HRMS)-based methods to examine the diversity of fatty acyl moieties attached to different residues in the *C. elegans* proteome. Strikingly, we found that *C. elegans* employs highly distinct sets of fatty acids for cysteine *S*-, lysine *N*-, and serine *O*-acylation, dominated by monomethyl branched fatty acids (mmBCFAs), specifically 15-methylhexadecanoic acid (isomargaric acid, isoC17:0) for cysteine *S*-acylation and 13-methyltetradecanoic acid (isoC15:0) for lysine *N*-acylation, in addition to smaller amounts of straight-chain saturated, monounsaturated, and polyunsaturated fatty acids. To gain insight into the specificity of fatty acyl attachment at the individual protein level, we performed large-scale proteomic profiling of *C. elegans* *S*- and *N*/*O*-fatty acylated proteins via copper(I)-catalyzed alkyne-azide cycloaddition (CuAAC) using a bioorthogonal alkyne analog of isoC17:0, Alk-C17i, along with two straight-chain alkyne probes, Alk-C16 and Alk-C18. The proteomics results demonstrated unexpected specificity of protein fatty acylation toward utilization of different fatty acids at both the protein and amino acid levels.

Results

Fatty Acylation Profiles of Different Amino Acid Residues in *C. elegans*. To comprehensively profile the chemical diversity of acyl groups attached to protein cysteine, N-terminal glycine, lysine, and serine residues, we used two strategies to distinguish different types of fatty acylation based on their chemical reactivity and stability: i) hydroxylamine treatment at neutral pH to survey for *S*-acylation (16, 23) and ii) protein enzymatic hydrolysis followed by analysis of fatty acyl-conjugated amino acids to profile hydroxylamine-resistant acylations (24–26) (Fig. 1*A*). Based on testing an *O*-acylated model substrate and literature precedent (*SI Appendix*, Fig. S1) (27), we expect that, in addition to *N*-acylation of glycine and lysine, the generally much less abundant *O*-acylation of serine is also hydroxylamine-resistant under our conditions.

To enable an unbiased survey of *S*-acylation patterns, including detection of unexpected or uncommon acyl moieties, we combined proteome-wide *S*-acyl capture using hydroxylamine with untargeted metabolomics and stable isotope labeling. For this purpose, proteome samples were extensively purified (*Materials and Methods*) to remove potentially confounding lipid derivatives and then incubated with stable isotope ^{15}N-labeled hydroxylamine or regular hydroxylamine (mostly ^{14}N), converting thioester modifications into ^{15}N- or ^{14}N-hydroxamic acids (HACs) that were analyzed by high-performance liquid chromatography (HPLC) coupled to HRMS (23). Comparative analysis of the resulting data for ^{15}N- and ^{14}N-hydroxylamine-treated samples using the XCMS and Metaboseek platforms (28) revealed diverse fatty acyl-derived HACs representing the corresponding protein cysteine *S*-acylations (Fig. 1*A*). Unexpectedly, an odd-chain fatty HAC feature, C17:0-HAC, was identified as the by far predominant species, accounting for more than 80% of the detected HACs, in addition to smaller amounts of C16:0-HAC, C18:0-HAC, and C18:1-HAC, which have been reported as predominant *S*-acyl modifications in other organisms (16), as well as trace amounts of C14:0-HAC, C15:0-HAC, C18:2-HAC, and C20:5-HAC (Fig. 1*B* and *SI Appendix*, Fig. S2*A*). Chromatographic profiling of synthetic HAC standards revealed that protein-derived C17:0-HAC represents almost exclusively the mmBCFA derivative, isoC17:0-HAC (Fig. 1*C*). In addition to a broad range of straight-chain fatty acids, *C. elegans* lipid profiles are known to include the mmBCFAs isoC15:0 and isoC17:0, as well as much smaller amounts of anteisoC15:0 and anteisoC17:0 (23, 29, 30), which are derived from endogenous branched-chain amino acid catabolism (31). Our results show that isoC17:0 is selectively recruited for protein *S*-acylation.

To profile protein *N*- and *O*-acylation on glycine, lysine, and serine residues, we employed previously developed strategies based on enzymatic protein hydrolysis followed by HPLC-HRMS analysis of the resulting acylated amino acids (24, 25) (Fig. 1*A*). To enrich for lipidated proteins, we isolated the membrane-associated protein fraction. Following protease and peptidase treatment, the resulting mixture of amino acids and derivatives was analyzed by HPLC-HRMS/MS for glycine, lysine, and serine acylated with common long-chain fatty acids (Fig. 1*A* and *SI Appendix*, Table S1). Synthetic standards of representative fatty acyl-amino acid conjugates were prepared as references for comparison of retention times and MS2 fragmentation patterns. Consistent with previous studies in multiple organisms (15, 32, 33), we found that N-terminal glycine was almost exclusively myristoylated (C14:0). C14:0-acylated glycine was over 100-fold more abundant than *N*-acyl-glycine conjugates with other fatty acids (C13:0, C15:0, and C16:0) (Fig. 1*D* and *SI Appendix*, Fig. S2*B*). In contrast, lysine residues were predominantly acylated with two mmBCFAs, isoC15:0 and isoC17:0 (Fig. 1*E* and *SI Appendix*, Fig. S2*C*). The lysine *N*-acylation profile was thus also distinct from that of cysteine *S*-acylation, as isoC15:0 was most abundant among lysine fatty acylations, whereas cysteine was predominantly acylated with isoC17:0 and only trace amounts of isoC15:0-acylated cysteine were detected. Yet another profile was observed for serine, which was found to be acylated with a broad range of fatty acyl moieties [C14 to C18, including the polyunsaturated eicosapentaenoic acid (EPA, C20:5)] (Fig. 1*F* and *SI Appendix*, Fig. S2 *D* and *E*). EPA *N*-acylation was also observed for lysine (Fig. 1*E* and *SI Appendix*, Fig. S2*F*), whereas *S*-acylation-derived EPA-HAC as well as EPA-acylated glycine were largely absent (Fig. 1 *B* and *C*). Collectively, these observations demonstrated that different amino acid residues exhibit highly specific fatty acylation profiles.

Development of a Clickable isoC17:0 Probe. The striking preference of the mmBCFA isoC17:0 for protein cysteine acylation led us to examine whether a bioorthogonal mimic of isoC17:0 could be used to probe cysteine *S*-acylation and acyl group preference at the protein level. We were further motivated to probe the role of cysteine *S*-acylation with isoC17:0 by the previous finding that supplementation of this mmBCFA could rescue a poorly understood developmental arrest phenotype of *C. elegans* lacking the biosynthetic gene for isoC17:0 and isoC15:0 (29). We thus designed a click chemistry–capable mimic of isoC17:0, named Alk-C17i, in which one of the terminal methyl groups of isoC17:0 is replaced with an acetylene moiety, which is roughly similar in size (Fig. 2*A*). Therefore, we anticipated that *C. elegans* would incorporate Alk-C17i in place of isoC17:0, enabling the use of click-chemistry to potentially enrich and characterize *S*-acylated proteins (Fig. 2*B*) (34). Synthesis of Alk-C17i was achieved via addition of a methyl group to the carbonyl of 15-hydroxypentadecanoic acid lactone (**1**) to form a methyl ketone (35), which following protection of the hydroxyl group with *tert*-butyldimethylsilyl chloride was subjected to Cu(I)-catalyzed cross-coupling with triisopropylsilyl acetylene to introduce the alkyne moiety at the terminal methyl branched position (36), finishing construction of the carbon backbone to give intermediate **4**. After a simultaneous deprotection of hydroxyl and alkyne groups, oxidation of the primary alcohol in intermediate **5** yielded the final product, Alk-C17i (Fig. 2*C*).

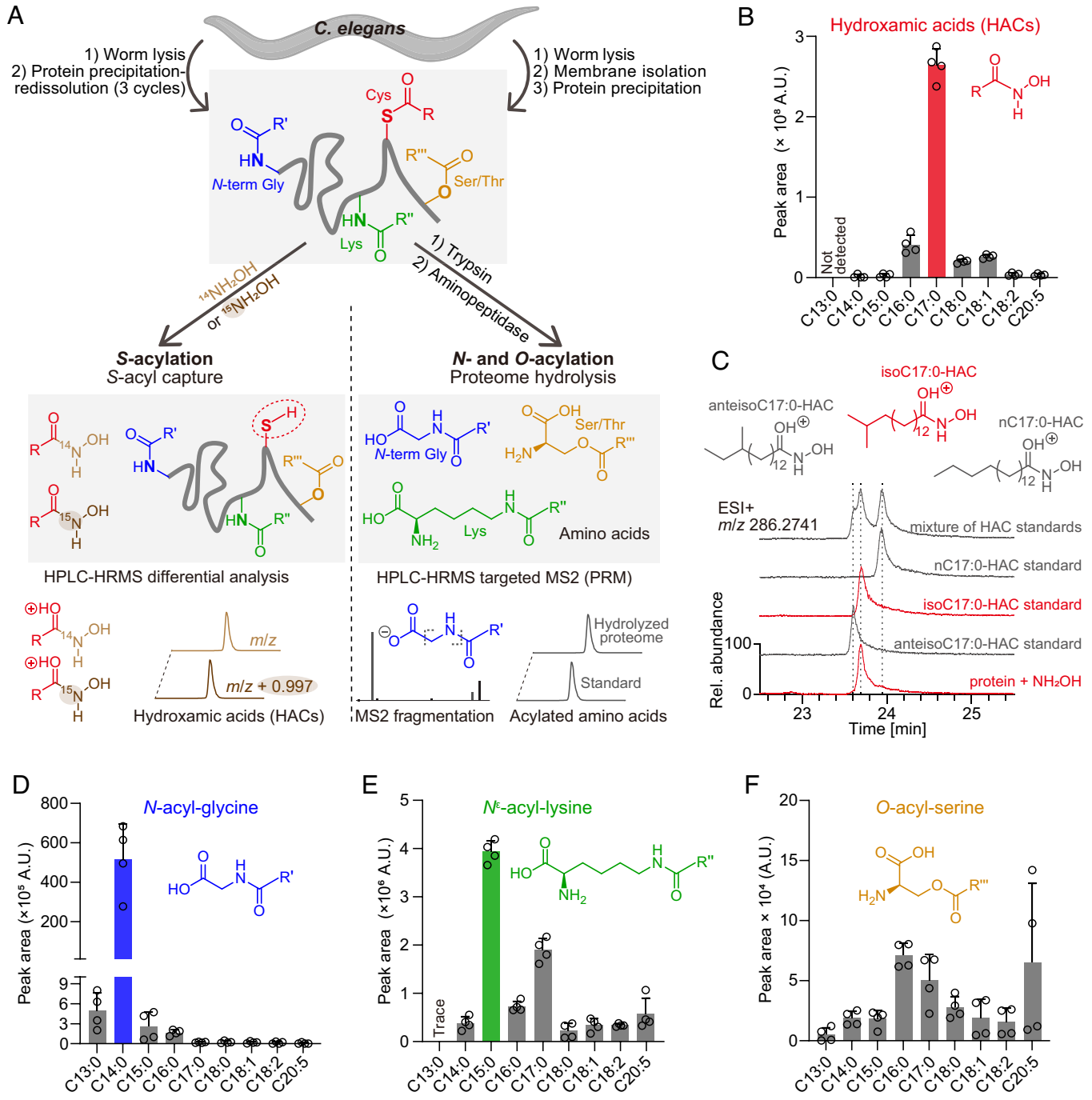

Fig. 1. Fatty acylation profiles of different amino acid residues in *C. elegans*. (*A*) Workflow of hydroxylamine *S*-acyl trapping for identification of cysteine acylation (*Left*) and protein enzymatic hydrolysis for profile of glycine (N-terminal), lysine, and serine fatty acylation (*Right*). (*B*) Peak area of fatty hydroxamic acids (HACs) derived from *S*-acylated proteins in *C. elegans*. n = 4. (*C*) Chromatographic profiles of C17:0-HAC standards demonstrate that the abundant C17:0-HAC in (*B*) is mostly isoC17:0-HAC. ESI, electrospray ionization. (*D*–*F*) Peak area of *N*-fatty acyl-glycines ($[M-H]^-$, (D)), N^{ε}-acyl-lysines ($[M+H]^+$, (E)), and *O*-acyl-serines ($[M-H]^-$, (F)) derived from enzymatic hydrolysis of *C. elegans* membrane fractions. n = 4. Data are mean ± SD in *B* and *D*–*F*.

Next, we asked whether our probe, Alk-C17i, could functionally replace isoC17:0. In *C. elegans*, the enzyme ELO-5 is responsible for elongation of isoC13:0-CoA to isoC15:0-CoA, which can be further elongated to isoC17:0-CoA by ELO-5 or ELO-6 (Fig. 2*D*) (21, 29). Deletion of *elo-5* results in developmental arrest at the first larval stage (L1 arrest) (29), which we confirmed can be rescued by dietary supplementation with isoC15:0 or isoC17:0 (Fig. 2*E* and *SI Appendix*, Fig. S3*A*). To clarify whether the synthesized probe Alk-C17i can compensate for lack of isoC17:0, we tested whether supplementation with Alk-C17i can rescue the L1 arrest phenotype of *elo-5* knockout worms in the same manner as isoC17:0. We found Alk-C17i fully rescued L1 arrest of *elo-5* mutant worms, whereas straight-chain terminal alkyne-containing fatty acids Alk-C16 or Alk-C18 had no effect (Fig. 2*E* and *SI Appendix*, Fig. S3*A*).

We then examined the incorporation of Alk-C17i into worm bodies and proteins using CuAAC with fluorophore-azide conjugates (Fig. 2*B*). Fluorescence microscopy images of Alk-C17i-fed *elo-5* mutant worms that were fixed and clicked with Cy3-azide showed that worms incorporated the alkyne (*SI Appendix*, Fig. S3*B*). In-gel

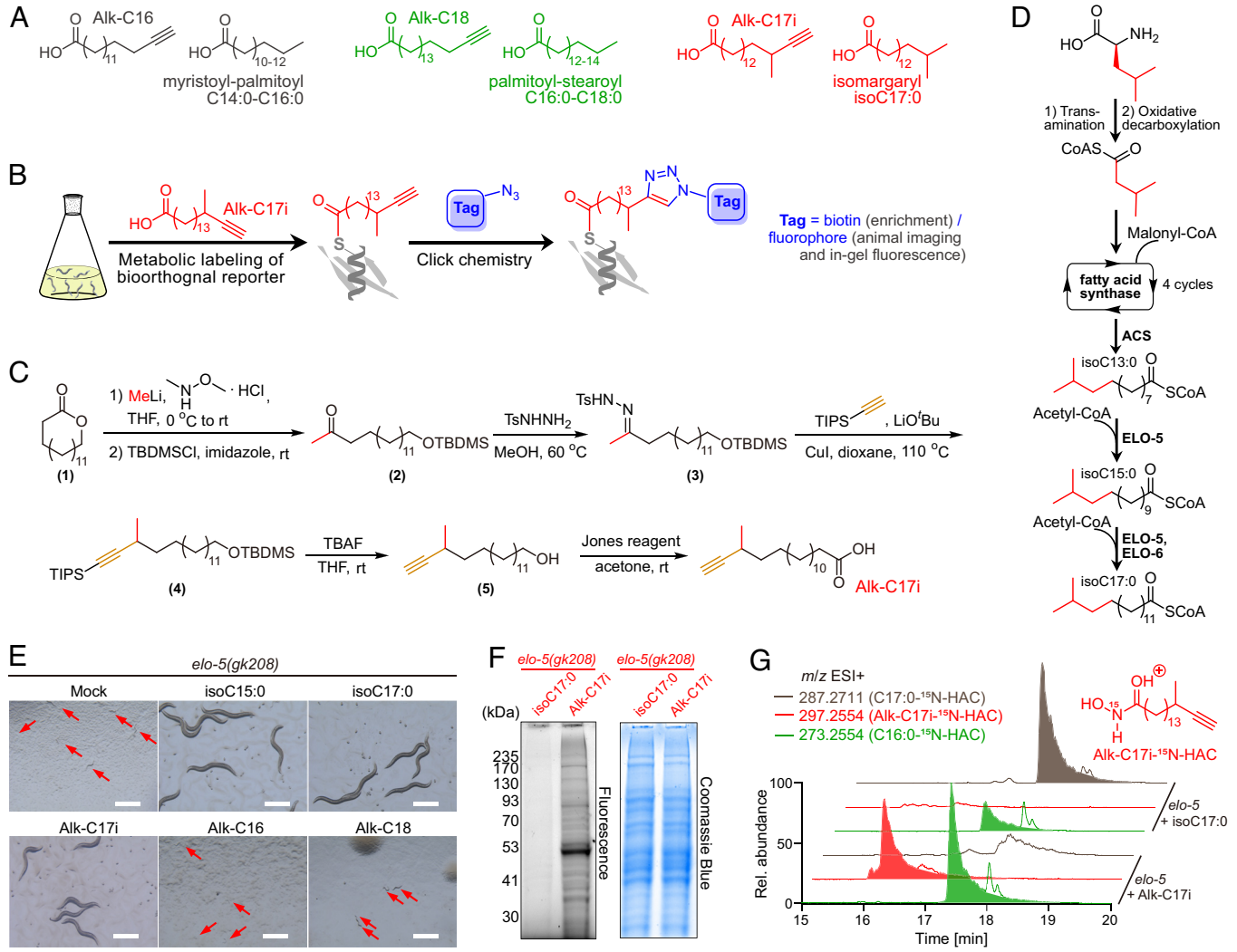

Fig. 2. Development of a clickable isoC17:0 probe. (*A*) Structures of alkyne fatty acids and the natural fatty acids they mimic. (*B*) Metabolic labeling and click chemistry with Alk-C17i. (*C*) Scheme of chemical synthesis of Alk17i. (*D*) Scheme of biosynthesis of isoC17:0 in *C. elegans*. (*E*) Representative images of synchronized *elo-5* KO larvae treated with different compounds after 72 h. isoC15:0, isoC17:0, and Alk-C17i rescued the development arrest phenotype of *elo-5* KO mutants, whereas Alk-C16 or Alk-C18 did not. (Scale bar: 0.5 mm.) (*F*) In-gel fluorescence of isoC17:0 (no alkyne control) or Alk-C17i-treated *elo-5* KO *C. elegans* proteins that had been clicked with TAMRA-azide and resolved by sodium dodecyl sulfate–polyacrylamide gel electrophoresis (SDS-PAGE). (*G*) Extracted ion chromatograms of HACs derived from $^{15}NH_2OH$ labeling of proteins isolated from isoC17:0- or Alk-C17i-fed *elo-5* mutant worms demonstrate incorporation of Alk-C17i onto protein cystine residues. (*E*–*G*) Compound concentration 375 μM.

fluorescence of TAMRA-azide clicked proteins extracted from Alk-C17i-fed *elo-5* mutant *C. elegans* revealed extensive TAMRA labeling, demonstrating Alk-C17i was incorporated onto proteins (Fig. 2*F*). Moreover, hydroxylamine labeling of proteins isolated and purified from Alk-C17i-treated *elo-5* mutant animals revealed robust incorporation of Alk-C17i on cysteine residues (Fig. 2*G*). Notably, *S*-acylation with straight-chain C16:0 increased in Alk-C17i-supplemented *elo-5* mutants compared to unsupplemented wildtype (WT) animals (Figs. 1*B* and 2*G*), suggesting that Alk-C17i is less preferred for *S*-acylation than endogenous isoC17:0, due to the non-natural alkyne moiety in Alk-C17i or lower bioavailability of the supplemented compound relative to endogenously produced isoC17:0. Alk-C15i-HAC and Alk-C13i-HAC that could be derived from chain-shortening of Alk-C17i via β-oxidation were not detected (*SI Appendix*, Fig. S3*C*). These results indicate that Alk-C17i can functionally replace isoC17:0 and thus may offer the opportunity to broadly profile *S*-acylated proteins in *C. elegans* bearing isoC17:0.

Click Chemistry–Based Profiling of Protein Fatty Acylation. In preparation for enrichment experiments for profiling protein fatty acylation in WT adult *C. elegans*, we optimized click chemistry and metabolic labeling conditions. Since Alk-C17i bears acetylene at a tertiary carbon, which can lower the efficiency of CuAAC, we tested four different common Cu(I) ligands (*SI Appendix*, Fig. S4*A*), of which we chose tris((1-benzyl-4-triazolyl)methyl) amine, a ligand previously used for CuAAC with fatty acid alkyne probes (37, 38). Monitoring levels of TAMRA-azide-clicked proteins via in-gel fluorescence, we found that 4 to 7 h of probe feeding in WT animals accomplished maximal labeling, whereas longer labeling times were less effective, possibly due to metabolism of the probe (*SI Appendix*, Fig. S4*B*). Further, imaging suggested that labeling for 6 h was sufficient for distribution of the alkyne probes across the worm body (*SI Appendix*, Fig. S4*C*). Next, we tested for potential toxicity of the alkyne probes. We did not observe any effects on survival or development of young adult or adult animals for any of the three probes at up to 200 μM for 6 h (*SI Appendix*, Fig. S4*D*); however, continuous treatment from hatching with Alk-C16 significantly delayed development (IC50 12.9 μM), while the other two alkynes did not affect development at up to 100 μM (*SI Appendix*, Fig. S4*E*). For the

labeling experiments, we therefore selected 6-h treatment of young adult animals at 50 µM of alkyne probes, similar to probe concentrations used in other model systems (39).

To comprehensively profile protein fatty acylation and assess potential specificity of Alk-C17i attachment compared to straight-chain alkyne probes, we supplemented parallel cultures with Alk-C17i and the two straight-chain probes Alk-C16 or Alk-C18 (Fig. 3*A*). Membrane protein fractions of WT *C. elegans* treated with different alkyne probes or mock (solvent) were subjected to click chemistry with biotin azide. Samples were then divided into two portions, of which one was treated with hydroxylamine to cleave thioesters, to enable distinguishing *N*/*O*-acylated proteins from proteins that are exclusively *S*-acylated. Next, biotinylated proteins were enriched with streptavidin-conjugated agarose beads and digested for bottom–up proteomics.

Among the total of 3,528 identified proteins, candidates were classified as significantly fatty acylated if they were, on average, at least threefold enriched in samples derived from one of the three probes, compared to mock-supplemented control (at $P < 0.05$, shown for Alk-C17i in Fig. 3*B*, see *SI Appendix*, Fig. S5 for other probes). We then further classified proteins whose abundance in each replicate was at least threefold reduced by hydroxylamine treatment compared to samples not treated with hydroxylamine as primarily *S*-acylated (Fig. 3 *C* and *D* and *SI Appendix*, Fig. S5 *C* and *D*) (37). Conversely, proteins were classified as primarily *N*/*O*-acylated if their abundance was reduced less than 1.5-fold upon treatment with hydroxylamine (Fig. 3*D*). Remaining acylated proteins, i.e., proteins, whose abundance was changed more than 1.5-fold but less than threefold, were considered as *S*-acylated, *N*/*O*-acylated, or both *S*- and *N*/*O*-acylated (Fig. 3*D*).

Fatty Acylation Patterns Are Highly Conserved. Analysis of the proteomics results using the above criteria yielded 775 *S*-acylated proteins in samples from Alk-C17i-supplemented animals (Fig. 4*A* and *SI Appendix*, Table S2). Application of stricter fold-change requirements (i.e., >fivefold) led to a list of 432 *S*-acylated proteins (Fig. 4*A* and *SI Appendix*, Table S2). Analogous data filtration yielded 766 and 375 *S*-acylated proteins for the Alk-C16- and Alk-C18-supplemented animals, respectively (Fig. 4*B* and *SI Appendix*, Table S2). A total of 1,013 *S*-acylated proteins were identified, many of which were labeled by more than one alkyne probe (Fig. 4*B*).

The overall number of *S*-acylated candidates we identified in *C. elegans* is similar to results from previous profiling experiments in other model systems (40, 41). Significantly, for 88% of *S*-acylated *C. elegans* proteins that have close orthologs in other organisms (defined by the SwissPalm database, https://swisspalm.org/), the corresponding orthologs have previously been reported to be *S*-acylated (Fig. 4*C* and *SI Appendix*, Table S3) (42), demonstrating a high degree of conservation of *S*-acylation patterns. Gene ontology biological process enrichment of the detected *S*-acylated proteins revealed functional classes, e.g., small GTPase

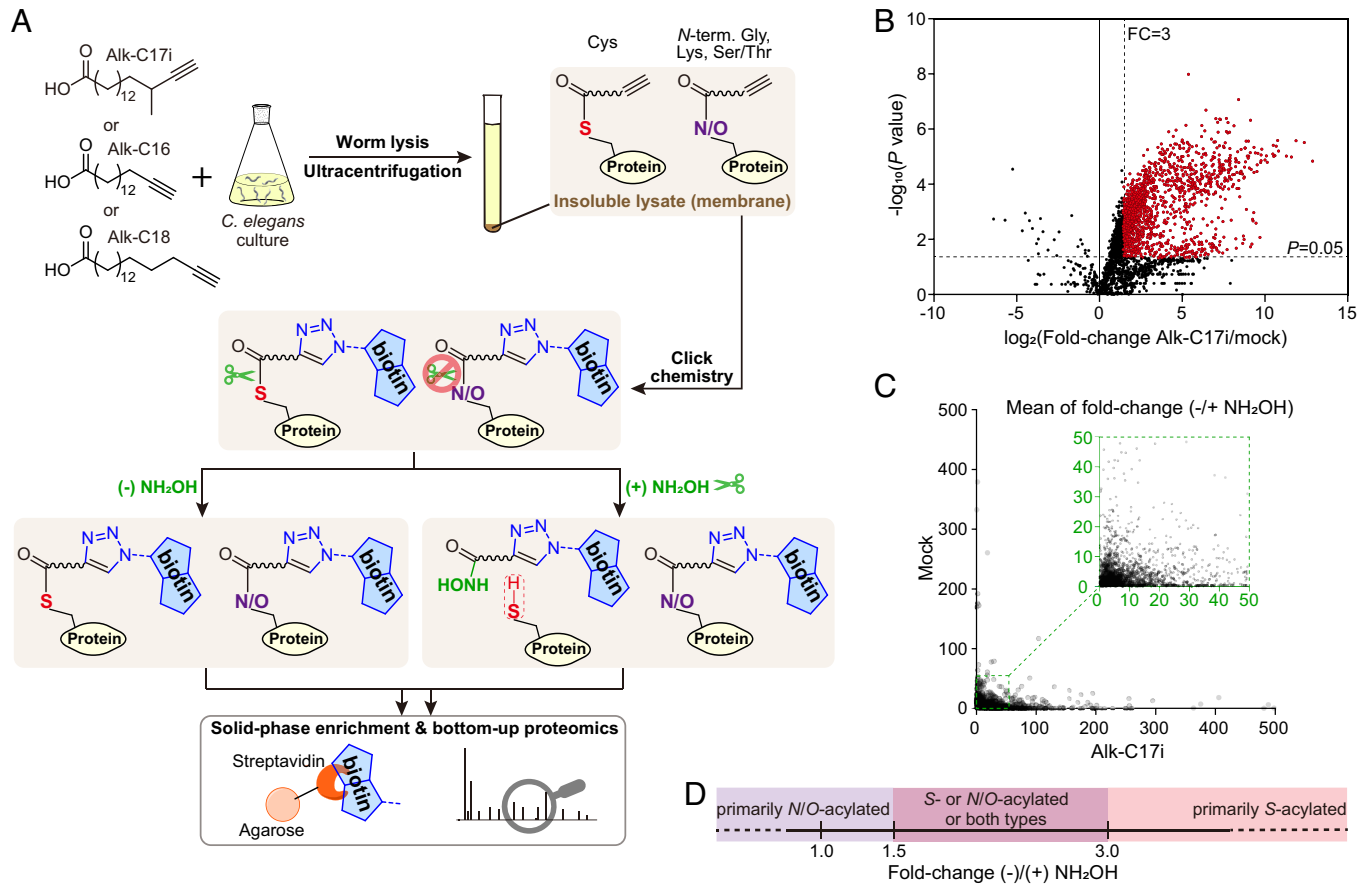

Fig. 3. Click chemistry–based profiling of protein fatty acylation in *C. elegans*. (*A*) Schematic application of alkyne fatty acids for enrichment and proteomics characterization of *S*- and *N*/*O*-fatty acylated proteins. (*B*) Volcano plot comparison of protein abundances from Alk-C17i- or mock-treated worms after CuAAC and bead enrichment. DMSO, n = 3; Alk-C17i, n = 4. (*C*) *x*, *y*-scatter plot depiction of protein intensity changes of plus- over minus-hydroxylamine samples from Alk-C17i- and mock-treated worms. Plus-hydroxylamine data were normalized by a factor that total intensities from plus- or minus-hydroxylamine mock-treated samples are identical. Mock, n = 3; Alk-C17i, n = 4. (*D*) Classification of proteins into primarily *S*-acylated or primarily *N*/*O*-acylated based on the fold-change of intensities upon hydroxylamine treatment.

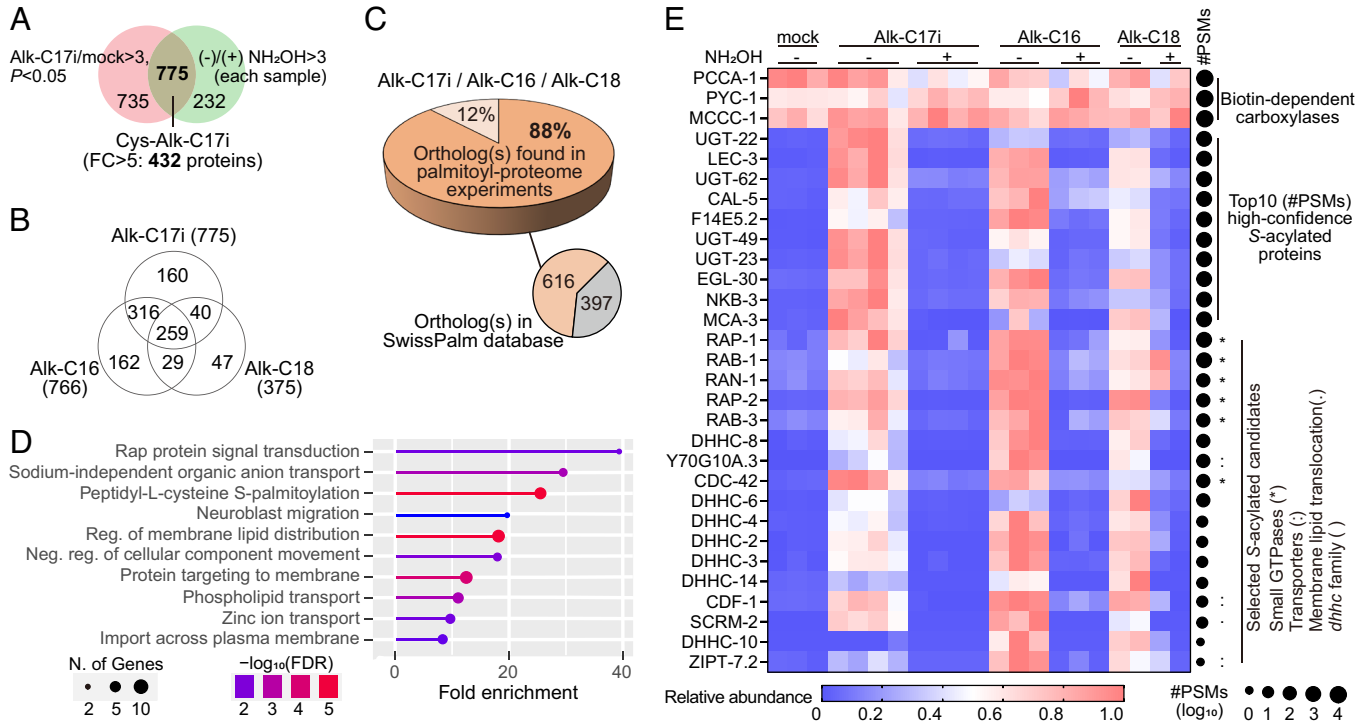

Fig. 4. Profiling of protein *S*-fatty acylation in *C. elegans*. (*A*) Overlap of Alk-C17i-enriched and hydroxylamine-cleavable proteins are cysteine isoC17:0-modified candidate proteins. FC, fold-change in both filters. (*B*) Number of *S*-acylated protein candidates identified using the three probes. Alk-C17i, n = 4; Alk-C16, n = 3; Alk-C18, n = 2. (*C*) Comparison of identified *C. elegans S*-acylated proteins with existing *S*-acylation data in the SwissPalm database. 616 of the 1,013 *S*-acylated *C. elegans* proteins have annotated orthologs in at least one of the species used in the SwissPalm-documented *S*-acyl-proteome experiments (91 experiments with 12 organisms; no experiments with *C. elegans* have been published). Orthologs of 88% of these 616 *C. elegans* proteins have been found in previous *S*-acyl-proteome experiments. (*D*) Biological process gene ontology analysis for *C. elegans S*-acylated proteins (Alk/mock > 5 and (−)/(+) NH_2OH > 5 in least one probe group). (*E*) Heat map of abundances of selected proteins including biotin-dependent carboxylases and *S*-acylated candidates. #PSMs, number of peptide spectrum matches in all samples.

signal transduction, metabolite transport, protein *S*-acyl transfer, (Fig. 4 *D* and *E* and *SI Appendix*, Fig. S7*A*), for which *S*-acylation (usually palmitoylation) is well known from mammalian systems. Most identified *S*-acylated proteins are presumed to localize to the intracellular organelle membranes, in addition to proteins localized at intercellular connections (*SI Appendix*, Fig. S7*B*).

Conversely, a total of 510 *N*- or *O*-fatty acylated proteins were identified across the three different alkyne probes using the above criteria (Fig. 5*A* and *SI Appendix*, Table S4). Notably, the numbers of *N*/*O*-acylated proteins identified in samples from animals supplemented with the straight-chain probes, Alk-C16 and Alk-C18 (333 and 336 proteins, respectively), were much larger than for Alk-C17i-supplemented animals (42 proteins, Fig. 5*A*). Gene ontology enrichment analysis for *N*- or *O*-fatty acylated proteins revealed membrane related processes as well as RNA processing and energy metabolism (Fig. 5*B* and *SI Appendix*, Fig. S8). Due to a lack of comprehensive global profiling databases for glycine, lysine, serine, and threonine fatty acylated proteins, we examined the data of highly conserved orthologs of several validated human proteins bearing N-terminal glycine myristoylation or lysine fatty acylation in a targeted manner, including ADP ribosylation factors (43, 44), Golgi reassembly stacking proteins (45, 46), serine hydroxymethyltransferase (47), Rho guanosine triphosphatase (GTPase) (48, 49), etc. In this targeted examination, we found that all *C. elegans* proteins for which the human orthologs have been found to be glycine *N*-myristoylated were in our list of *N*- or *O*-fatty acylated proteins, and, significantly, that they were only labeled by Alk-C16 but not by the longer-chain probes Alk-C18 or Alk-C17i (Fig. 5*C*), consistent with our finding that C14:0 is strongly preferred for glycine *N*-acylation (Fig. 1*D*). ARF-6, MEL-32, and RHO-1, orthologs of known human lysine fatty acylated proteins ARF6 (50), SHMT2 (47), and RHOA (48, 49), respectively, were significantly enriched in the alkyne-treated groups but were not classified into either *S*-acylated or *N*/*O*-acylated, possibly due to co-presence of lysine and cysteine fatty acylations, as also reported for their human orthologs (Fig. 5*C*). ARF-6 and MEL-32 are two examples of the 1,291 proteins in our dataset that were significantly enriched by labeling with one of the alkyne probes but could not be classified as primarily *S*- or *N*/*O*-modified (*SI Appendix*, Table S5).

Validation of *C. elegans* Fatty Acylated Proteins. Next, we selected five proteins for validation of their fatty acylation type based on conservation, availability of antibodies, or predicted modification sites. This included the small GTPase RAN-1 and the ADP-ribosylation factor ARF-1.2 that are highly conserved from *C. elegans* to mammals. Immunoblots of RAN-1 and ARF-1.2 in the streptavidin pull-down samples derived from Alk-C16 labeling, click chemistry with biotin azide, and hydroxylamine *S*-acyl cleavage validated that RAN-1 is primarily *S*-acylated (Figs. 4*E* and 6*A*), and ARF-1.2 is primarily *N*/*O*-acylated (Figs. 5*C* and 6*B* and see *SI Appendix*, Fig. S9 for antibody validations), reflecting the acylation pattern of their mammalian homologs. Similarly, we validated that the ortholog of human SCRIB (scribble planar cell polarity protein) LET-413 is primarily *S*-acylated (Fig. 6*C*), and the neuroglian SAX-7 is primarily *N*/*O*-acylated (Fig. 6*D*), using antibodies previously developed for these *C. elegans* proteins (51). In addition, we uncovered C254 as the predominant *S*-acylation site in the two-Ig domain protein ZIG-1, as demonstrated by the presence of a streptavidin pull-down signal from the N-terminal *3xflag* CRISPR-Cas9 knock-in

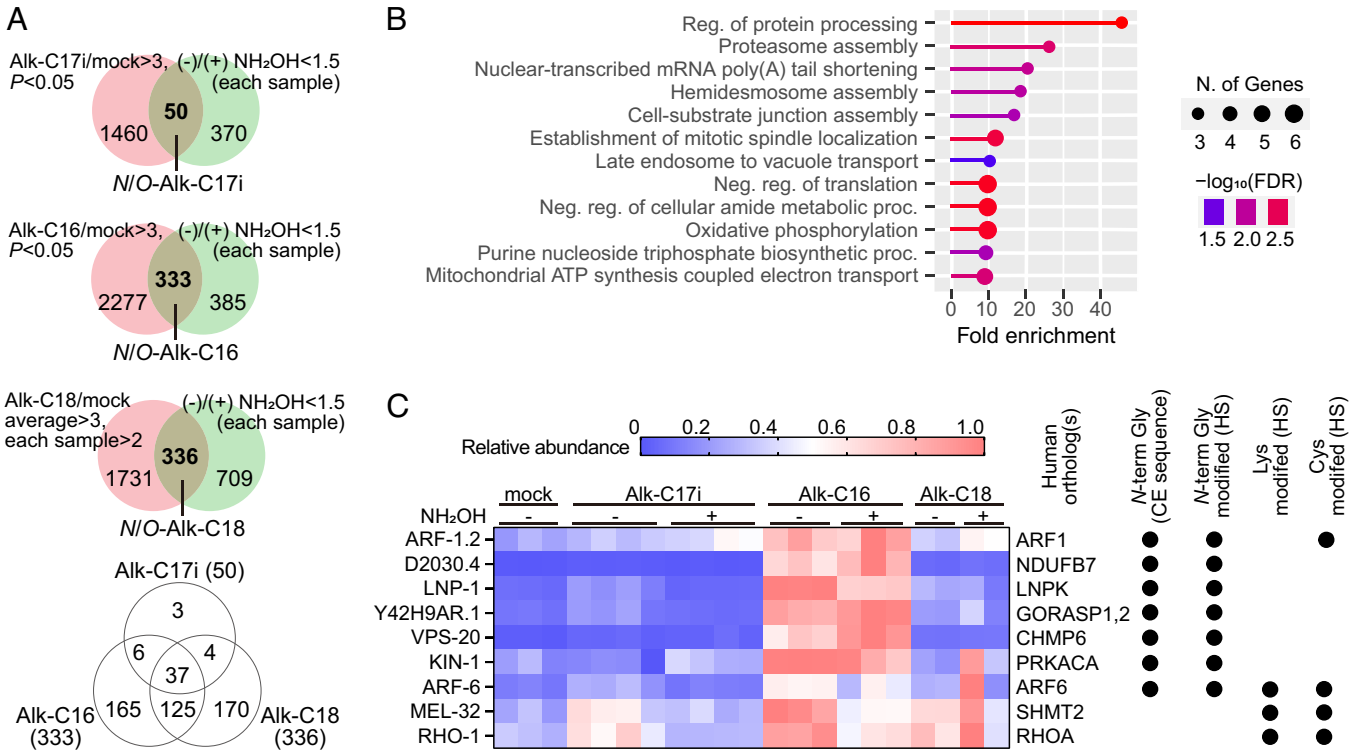

Fig. 5. Profiling of protein *N*- and *O*-fatty acylation in *C. elegans*. (*A*) Overlap of alkyne-enriched and hydroxylamine-resistant proteins is *N*/*O*-fatty acyl-modified candidate proteins. Criteria for filtration are shown for each Venn diagram. Mock, n = 3; Alk-C17i, n = 4; Alk-C16, n = 3; Alk-C18, n = 2. (*B*) Biological process gene ontology analysis for *C. elegans N*/*O*-acylated proteins. (*C*) Heat map of abundances of selected proteins, including *N*/*O*-fatty acylated candidates that are orthologs of known human N-terminal glycine myristoylated proteins (*Top* six), and orthologs of known human lysine fatty acylated proteins (*Bottom* three). Cys modification data were retrieved from SwissPalm, filtering for entries with detection in more than 5 experiments (22 in total). Abbreviations: CE, *C. elegans*; HS, *H. sapiens*.

zig-1 mutant fed with alkyne fatty acid, which is absent in the corresponding C254A point mutant (Fig. 6*E* and *SI Appendix*, Fig. S10*A*). C254 is adjacent to the transmembrane helix of ZIG-1, and C254 is predicted to be *S*-acylated with high confidence by the machine learning-based algorithm, GPS-Palm (*SI Appendix*, Fig. S10*B*) (52). Taken together, these results confirm *S*- and *N*/*O*-acylation as indicated by our global proteomics profiling for all five selected proteins.

Specificity of Protein Fatty Acylation with Different Alkyne Probes. Despite a great overlap of proteins labeled by all three alkyne fatty acids, Alk-C17i was preferred over the two straight-chain alkyne probes for *S*-acylation (Fig. 4*B*) and disfavored for *N*/*O*-acylation (Fig. 5*A*). More than half of the intensity of total Alk-C17i-enriched proteins was derived from *S*-acylated candidates, whereas less than 5% were derived from *N*/*O*-acylated proteins. In contrast, the intensities from *S*-acylated and *N*/*O*-acylated proteins labeled by Alk-C16 or Alk-C18 were similar (within 1.5-fold difference) (Fig. 6*F*). Moreover, applying stricter criteria for filtration of *S*-acylated candidates (i.e., higher fold-change for both probe enrichment and hydroxylamine cleavage), resulted in a higher percentage of Alk-C17i-specific proteins among all *S*-acylated proteins (*SI Appendix*, Fig. S11). These results indicate that the iso-branched Alk-C17i to some extent recapitulates preferential *S*-acylation with endogenous isoC17:0.

We additionally observed highly preferential *S*-acylation of individual proteins by one of the three probes. Comparing abundances of individual proteins labeled with different probes, we found five and ten proteins that were highly preferentially labeled by Alk-C17i or Alk-C16, respectively (with more than 10-fold preference for either Alk-C17i vs. Alk-C16 or Alk-C16 vs. Alk-C17i labeling, Fig. 6 *G* and *H*). Among the five Alk-C17i-specific proteins are two members of cytochrome P450 family (CYP-35A4, CYP-14A3) (Fig. 6*H*). Moreover, the most abundant *S*-acylated proteins (Fig. 4*E*) include two UDP-glucuronosyltransferases (UGT-22, UGT-23) that are also preferentially modified by Alk-C17i (*SI Appendix*, Fig. S12). Proteins almost exclusively *S*-acylated with the straight-chain probes included the calcium-transporting ATPase PMR-1 and *S*-acyltransferase DHHC-10 (Fig. 6*H*). Given that our initial hydroxylamine-based profiling revealed that *S*-acylation is dominated by isoC17:0, the identification of specific proteins that are almost exclusively *S*-acylated with straight-chain alkyne probes was unexpected. To validate the preference for straight-chain alkynes by DHHC-10, we generated a transgenic *3xflag-dhhc-10* overexpression strain followed by feeding with the three different alkyne probes, click chemistry, and streptavidin pull-down. Consistent with the proteomics results, the western blot showed that DHHC-10 was only modified by straight-chain alkynes, but not by the methyl branched Alk-C17i (Fig. 6*I* and *SI Appendix*, Fig. S13). Taken together, our results reveal a high level of specificity of *S*-acylation for a small subset of proteins, in addition to the utilization of different fatty acid profiles for different amino acid residues.

Discussion

Using *C. elegans* as a model and a set of click chemistry–capable fatty acid probes, we uncovered unexpected diversity and specificity of protein fatty acylation. Our untargeted screening revealed utilization of distinct profiles of fatty acids for acylation of different amino acid residues. We established that mmBCFAs dominate both cysteine and lysine acylation profiles, whereby cysteine

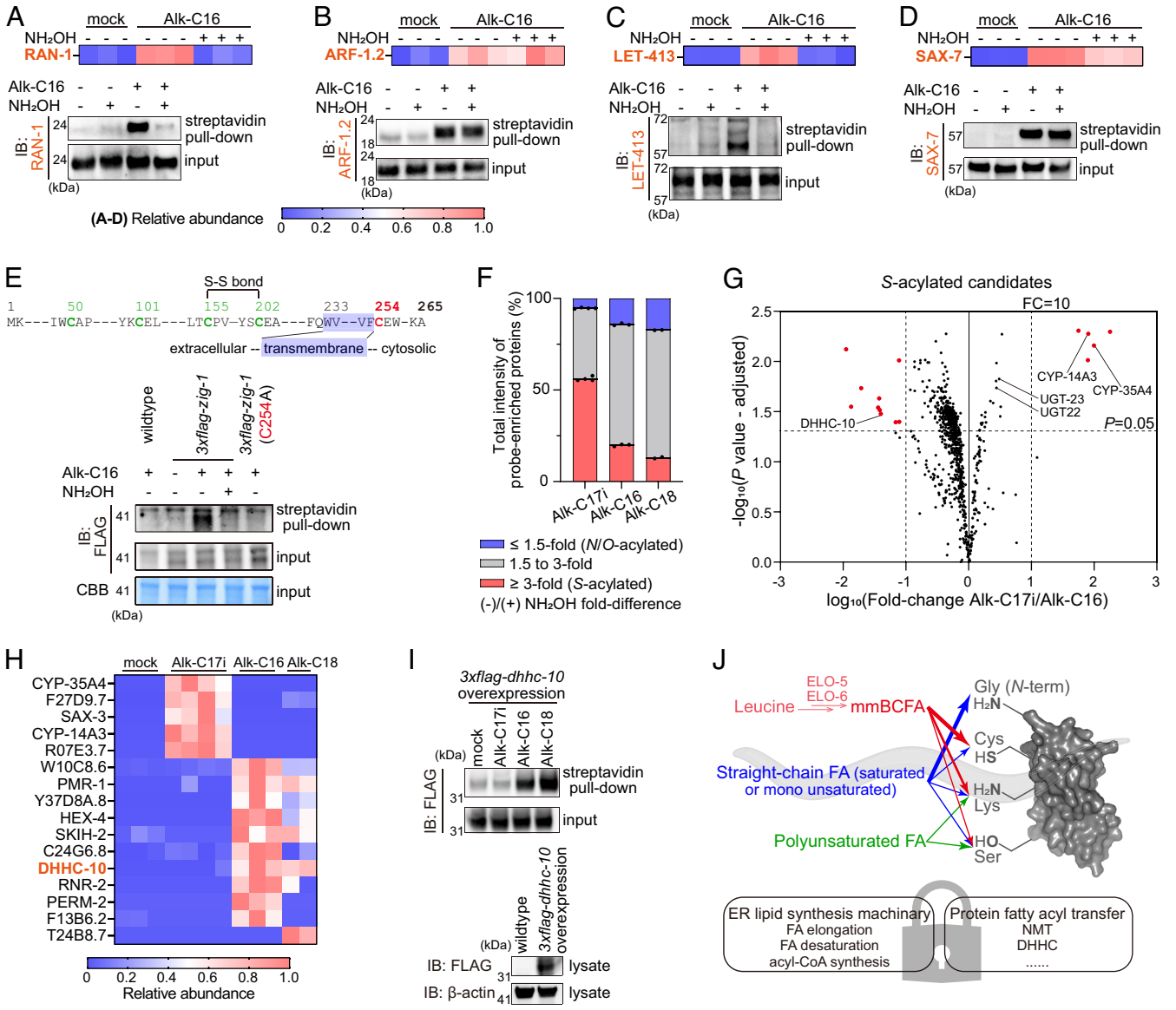

Fig. 6. Validation of *C. elegans* fatty acylated proteins and specificity of protein fatty acylation with different alkyne probes. (*A*–*D*) Immunoblot detection of selected fatty acylated proteins in streptavidin pull-down samples derived from Alk-C16 labeling, click chemistry with biotin azide, and subsequent hydroxylamine *S*-acyl cleavage. Same workflow as Fig. 3*A* except for using western blot as readout. The patterns in the immunoblots are consistent with the proteomics profiling results (heat map strips shown on *Top* of each panel). (*E*) Validation of the predicted *S*-acylation site (C254A) in ZIG-1. C254 is the residue number in WT protein. (*F*) Percentage of the total intensity of hydroxylamine-cleavable (*S*-acylated) and hydroxylamine-resistant (*N*/*O*-acylated) proteins among the total intensity of alkyne-enriched proteins. Alk-C17i, n = 4; Alk-C16, n = 3; Alk-C18, n = 2. (*G*) Volcano plot comparison of abundances of *S*-acylated proteins labeled by Alk-C17i or Alk-C16. *P* values were adjusted using the Benjamini-Hochberg procedure. Alk-C17i, n = 4; Alk-C16, n = 3. (*H*) Heat map of abundances of *S*-acylated proteins that were labeled with more than 10-fold specificity by Alk-C17i or Alk-C16 (red dots in *G*) as well as a protein that was Alk-C18-specifically labeled relative to Alk-C17i and Alk-C16. (*I*) Validation of preferential acylation of DHHC-10 with straight-chain alkyne fatty acids. (*J*) Summary of protein fatty acylation specificity and model for potential mechanisms coupling ER lipid synthesis machinery and protein fatty acyl transfer.

acylation is dominated by isoC17:0, while lysine is acylated by a broader profile of fatty acids, with isoC15:0 being most abundant. These mmBCFAs are derived from leucine catabolism (21), indicating that protein acylation and especially cysteine *S*-acylation depend on this specific branch of endogenous fatty acid metabolism. Although the mammalian fatty acyl elongation machinery does not produce long-chain mmBCFAs, mmBCFAs are present in food and produced by the gut microbiome, and mmBCFAs from both sources have been shown to have significant effects of physiology and disease in mouse models (53). Our work uncovers an example of abundant protein post-translational modification with mmBCFAs, which may motivate investigation of potential mmBCFA acylation in mammalian and other systems. The bioorthogonal tool developed in this study (i.e., Alk-C17i) should be fully translatable to other models building on previous studies (37, 54).

In contrast, no preference for mmBCFAs was observed for protein N-terminal glycine fatty acylation or serine modification; instead, protein N-terminal glycine is almost exclusively myristoylated, whereas serine is acylated by a wider range of long-chain fatty acids, including the polyunsaturated fatty acid, EPA. To a lesser extent, EPA acylation was also observed for lysine, suggesting that polyunsaturated fatty acid metabolism may broadly feed back onto protein acylation. With regard to our list of *N*/*O*-acylated protein candidates, it should be noted that *O*-fatty acylation is comparatively rare in eukaryotes (1), and thus, most hydroxylamine-resistant proteins we detected likely represent *N*-acylated species. Further, although our

hydroxylamine treatment conditions should generally leave *O*-acylation intact, we cannot exclude that some *O*-ester bonds may be cleaved by hydroxylamine, e.g., as a result of a specific chemical microenvironment.

The diversity of fatty acyl moieties utilized for serine and lysine acylation suggests that subsets of proteins may be preferentially acylated with specific fatty acids. Notably, we found that even in the case of cysteine *S*-acylation, which predominantly utilizes isoC17:0, a subset of proteins was almost exclusively acylated with the straight-chain probes, suggesting that these proteins are primarily *S*-acylated with palmitic or stearic acid and not isoC17:0, which we validated for the case of the *S*-acyltransferase DHHC-10. Importantly, building evidence indicates that protein fatty acylation by specific fatty acids can dramatically affect function (55). For example, stearoylation (not common palmitoylation) of human transferrin receptor TFR1 inhibits its activation of JNK signaling and promotes mitochondrial fusion (56). Additional examples include specific *O*-palmitoleylation controlling secretion of Wnt proteins (12) and preferential auto-*S*-acylation of the transcription factor RFX3 with stearic acid and oleic acid (57). The preferential utilization of isoC17:0 for cysteine *S*-acylation in *C. elegans* may explain the still poorly understood (58–60) requirement of isoC17:0 for normal larval development. Supplementation with Alk-C17i rescued the larval arrest phenotype of *elo-5* knockout animals, and thus our list of Alk-C17i-*S*-acylated proteins may include candidates that merit further study for their potential relevance for larval development. Moreover, Alk-C17i can also serve as a tool for future investigation of mmBCFA metabolism on both the metabolite and protein levels, combining click chemistry with mass spectrometric approaches and solid-phase enrichment (61).

Specificity of fatty acid utilization for acylation of different amino acids could arise via a variety of mechanisms (Fig. 6*J*). Acyl transferases may exhibit specificity for fatty acyl-CoAs of specific chain length, degree of unsaturation, or presence of methyl branching. For example, in vitro studies demonstrated that some widely conserved glycine *N*-myristoyltransferases (NMTs) only transfer myristoyl but not palmitoyl (62). In contrast, the specificity of cysteine fatty acylation is less well understood. While the acyl binding groove of the human cysteine *S*-acyltransferase ZDHHC20 accommodates only fatty acyl moieties shorter or equal to 16 carbons (63), the residues responsible for closing this acyl binding groove are not present in the majority of human *S*-acyltransferases or *C. elegans* DHHCs. Similarly, structural constraints might explain our finding that DHHC-10 is preferentially acylated with straight-chain alkyne fatty acids, in contrast to other detected DHHCs in *C. elegans*. Specificity could also arise from association of acyl transferases with components of biosynthesis and transport of mmBCFAs or their CoA derivatives, as well as cell compartment-specific or otherwise localized enrichment. Such mechanisms may also explain the striking specificity of *S*-acylation of a small number of proteins with the straight-chain probe Alk-C16. For lysine fatty acylation, NMTs are the only so-far characterized eukaryotic acyl transferases (50, 64). Our results demonstrating distinct fatty acylation profiles for glycine and lysine residues in *C. elegans* suggest that additional enzymes and other mechanisms, as for cysteine *S*-acylation, contribute to lysine fatty acylation.

Although protein *S*-acyl diversity in mammalian models has been explored to a considerable extent (16, 17, 65), most previous work is not based on untargeted approaches, which, as we show here for *C. elegans*, can reveal unexpected fatty acyl moieties and specificity, including reliance on specific branches of fatty acid metabolism, e.g., isoC17:0 biosynthesis. Further, our work provides a global overview of lysine and serine *N*- and *O*-acyl moieties, complementing prior work on lysine (66) and serine (12) acylation profiles using purified individual proteins. Finally, our comprehensive analysis of *C. elegans* fatty acylated proteins, including identification of many conserved proteins that are acylated at the same type of residues as their homologs in other species, provides a resource for mechanistic studies of the roles of protein fatty acylation, including the residue- and protein-specific utilization of fatty acids.

Materials and Methods

Detailed methods are provided in *SI Appendix*.

Nematode and Bacterial Strains. *C. elegans* WT (N2) and the *elo-5* knockout strain VC410(*gk208*) were obtained from the Caenorhabditis Genetics Center (CGC). The N-terminal *3xflag* CRISPR-Cas9 knock-in *zig-1* mutant strain PHX8149 (*syb8149*), the C254A CRISPR-Cas9 point mutant of the *zig-1*(*syb8149*) strain PHX8254 (*syb8254*, C254 is the residue number in WT protein), and the *3xflag-dhhc-10* overexpression strain generated through X-ray-mediated integrated arrays were obtained from SunyBiotech (Fuzhou, China); see *SI Appendix* for sequence details. Bacterial strain *Escherichia coli* OP50 was obtained from CGC. Worms were maintained on petri dish plates containing nematode growth medium (NGM) coated with stationary-phase *E. coli* OP50 LB culture. Then, 50 μM of isoC15:0 or isoC17:0 was added to plates for maintaining the development of *elo-5* mutants.

Chemical Synthesis of Alk-C17i and Analytical Standards. See *SI Appendix*.

***C. elegans* Cultures.** To obtain large amounts of *C. elegans* for protein extraction, worms were grown in liquid culture as previously described (23). Synchronized L1 larvae were grown at ~280,000 animals per 100 mL S-complete media at 20 °C supplemented with 4 mL concentrated *E. coli* OP50 (1 g/mL) as food for 68 to 70 h before harvest for hydroxylamine (NH_2OH) treatment or 62 to 64 h before alkyne labeling.

$^{14}NH_2OH$- and $^{15}NH_2OH$-Treatment of *C. elegans* Proteome. Proteins from *C. elegans* lysates were purified through three cycles of methanol–chloroform protein precipitation, and the protein pellets were redissolved using a sodium dodecyl sulfate (SDS) buffer in between. The resulting protein pellets were resuspended in 0.1× PBS and aliquoted into three portions, which were treated with aqueous NaCl solution (0.19 M final, no NH_2OH control), $^{14}NH_2OH{\cdot}HCl$ aqueous solution (1.2% final, NaOH-neutralized), or $^{15}NH_2OH{\cdot}HCl$ solution (1.2% final, NaOH-neutralized). The samples were sonicated for 5 min, lyophilized, extracted with methanol, further concentrated, and resuspended in 100 μL of methanol for HPLC-HRMS analysis.

HPLC-HRMS Analyses of Small Molecules and Comparative Analysis to Identify NH_2OH-Labeled Compounds. See *SI Appendix* for HPLC-HRMS data acquisition methods using reversed-phase chromatography coupled to HRMS. Untargeted data analysis was performed as previously described using Metaboseek software (23, 28).

HPLC Separation of nC17:0-HAC, isoC17:0-HAC, and anteisoC17:0-HAC. The separation was performed on a Thermo Scientific Hypersil GOLD C18 column (150 × 2.1 mm, 1.9 μm particle size, 175 Å pore size) maintained at 40 °C with a flow rate of 0.5 mL/min. Solvent A: 0.1% formic acid in water; solvent B: 0.1% formic acid in acetonitrile. The A/B gradient was as follows: isocratic at 5% B for 3 min, linearly increasing to 75% B at 23 min, linearly increasing to 85% B at 30 min, linearly increasing to 100% B at 32 min, keeping at 100% B for 4 min, shifting back to 5% B in 0.1 min, and holding at 5% B until 40 min.

Exhaustive Digestion of *C. elegans* Membrane Proteins and HPLC-HRMS/MS Analysis of the Digest. The insoluble fraction (membrane enriched) of *C. elegans* lysate prepared in detergent-free lysis buffer was further extracted with a buffer containing 1% Triton X-100. Proteins were isolated by methanol–chloroform precipitation and redissolved in a urea buffer. Enzymatic digestion of 2.5 mg proteins was performed by sequential application of two enzymes, 25 μg

sequencing grade trypsin (Promega) and 2.5 units of aminopeptidase-M (Sigma-Aldrich) (26). Peptides resulted from trypsin digestion were desalted with C18 cartridges (Sep-Pak, Waters) before aminopeptidase treatment. Samples were resuspended in 70 μL methanol for liquid chromatography−tandem mass spectrometry (LC−MS/MS) analysis. See *SI Appendix*, Table S1 for a list of fatty acyl-amino acid conjugates, precursor *m/z* inclusion, analysis ESI polarity, MS/MS collision energy, and detected fragments. For quantification, the mass spectrometer was run on MS1 mode, peak area of $[M-H]^-$ ions was used for quantifications of glycine and serine conjugates, and peak area of $[M+H]^+$ ions was used for lysine conjugates.

***C. elegans* Development Assay.** To examine the developmental effect of fatty acid (derivative) supplementation, compound (isoC15:0, isoC17:0, Alk-C17i, Alk-C16, or Alk-C18) solution (dimethyl sulfoxide/ethanol/M9 buffer = 1/1/2, v/v/v) or solvent only was added to seeded NGM agar plates and allowed to diffuse overnight at 4 °C. Approximately thirty synchronized starved WT or *elo-5(gk208)* L1-stage animals were exposed to compounds on 35-mm plates for 64 h or 72 h at 20 °C, and then, developmental stages were examined.

Click Chemistry and Protein In-Gel Fluorescence. Click chemistry was performed at 37 °C for 2 h with lysates containing 0.4 mg protein that had been diluted in 0.4 mL lysis buffer (50 mM triethanolamine, 150 mM NaCl, and 4% SDS, pH 7.4) and reagents (30 μM tetramethylrhodamine (TAMRA)-azide, 12 μM tris(benzyltriazolylmethyl)amine, 303 μM tris(2-carboxyethyl)phosphine, and 303 μM $CuSO_4$). Proteins were purified by methanol–chloroform precipitation and were resolved via SDS-PAGE. Fluorescence was detected using a ChemiDoc MP imaging system (Bio-Rad).

Metabolic Labeling with Alkyne Fatty Acids and Enrichment of Fatty Acylated Proteins. Fatty acid alkyne probes (DMSO as control, Alk-C17i, Alk-C16, or Alk-C18, final concentration 50 μM) were added to the *C. elegans* cultures at 62 h from initiation of synchronized L1 growth in liquid media, and worms were allowed to grow for an additional 6 h. Protein extraction, click chemistry, hydroxylamine *S*-acyl cleavage, and streptavidin pull-down were performed as previously described (37).

Proteomic Analysis of Enriched Proteins. Streptavidin–agarose beads were sequentially washed by 0.2% SDS in PBS, 4 M urea in 0.25× PBS, PBS, high salt buffer (500 mM KCl and 20 mM Tris pH 7.5), and 20 mM Tris (pH 7.5) before protein on-bead digestion by trypsin (37). Peptides were analyzed by nanoLC−MS/MS; see *SI Appendix* for instrument methods. Protein identification and quantification were performed with Proteome Discoverer software (v 2.5, Thermo Fisher Scientific) using FASTA files retrieved from Uniprot (www.uniprot.org, UP000001940). The resulting table was zero-filled with a value of "1×10^3". Protein abundances in NH_2OH-treated samples were scaled to ensure that total intensities from NH_2OH-untreated and NH_2OH-treated mock-supplemented (no alkyne) samples are identical. Significance *P* values were calculated assuming two-tailed distributions and heteroscedasticity (unequal variance between groups), based on $\log_{10}$-transformed intensity (67). For comparison of abundances of proteins labeled by Alk-C17i or Alk-C16, *P* values were adjusted using the Benjamini–Hochberg procedure.

Cross-Species Palmitoyl-Proteome Comparison and Gene Ontology Analysis. Cross-species palmitoyl-proteome comparison was performed using the SwissPalm database (https://swisspalm.org), release 4 (2022–09–03) (42). Gene ontology analysis was performed with an online bioinformatics tool (bioinformatics.sdstate.edu/go/) (68).

Immunoblotting of Streptavidin-Enriched Proteins. Western blotting was performed using standard protocols; see *SI Appendix* for detailed procedures. Before the addition of streptavidin-agarose for pull-down, 4% of the sample was saved as "input". Antibodies used in this study and their dilution factors: Ran antibody (rabbit pAb, Cell Signaling Technology, #4462) 1:1,000, ARF1 antibody (rabbit mAb, recombinant, Invitrogen, SD2002) 1:1,000, LET-413 antibody (mouse mAb, Developmental Studies Hybridoma Bank, DSHB) 1:50, SAX-7 antibody (mouse mAb, DSHB) 1:50, ANTI-FLAG M2-HRP (mouse mAB, Sigma-Aldrich) 1:1,000, anti-β-actin-HRP (Santa Cruz Biotechnology, C4, sc-47778) 1:2,000, anti-rabbit-HRP (goat pAB, Promega) 1:2,000, and anti-mouse-HRP (goat pAB, Promega) 1:2,000. Use of antibodies produced for mammalian proteins had been validated using RNAi knockdown of *C. elegans* transcripts.

Data, Materials, and Software Availability. The raw MS files of proteomics experiments have been deposited in the MassIVE database; accession code MSV000093332 (https://massive.ucsd.edu/ProteoSAFe/dataset.jsp?task=d92e8fac06d24be793ffdccdc1ed7120) (69). The paper does not report any original code.

ACKNOWLEDGMENTS. We thank Tyler R. Bales and Kaidi Hu for technical assistance; Qiulin You for assistance in chemical synthesis; the CGC for *C. elegans* strains; and the laboratory of F.C.S. for advice and comments on the manuscript. Bacterial strains for RNAi experiments were a gift from Dr. Siu Sylvia Lee. This work made use of the Cornell University NMR Facility, which is supported, in part, by the NSF through MRI award CHE-1531632. This work was partly supported by the NIH (R01CA240529 to H.L.; R35 GM131877 to F.C.S.; and P40 OD010440 to CGC) and the NSF (2226270 to A.S).

Author affiliations: [a]Boyce Thompson Institute, Cornell University, Ithaca, NY 14853; [b]Department of Chemistry and Chemical Biology, Cornell University, Ithaca, NY 14853; [c]HHMI, Cornell University, Ithaca, NY 14853; and [d]Department of Molecular Biology and Genetics, Cornell University, Ithaca, NY 14853

1. H. Jiang *et al.*, Protein lipidation: Occurrence, mechanisms, biological functions, and enabling technologies. *Chem. Rev.* **118**, 919–988 (2018).
2. T. Peng, E. Thinon, H. C. Hang, Proteomic analysis of fatty-acylated proteins. *Curr. Opin. Chem. Biol.* **30**, 77–86 (2016).
3. T. Lanyon-Hogg, M. Faronato, R. A. Serwa, E. W. Tate, Dynamic protein acylation: New substrates, mechanisms, and drug targets. *Trends Biochem. Sci.* **42**, 566–581 (2017).
4. B. Chen, Y. Sun, J. Niu, G. K. Jarugumilli, X. Wu, Protein lipidation in cell signaling and diseases: Function, regulation, and therapeutic opportunities. *Cell Chem. Biol.* **25**, 817–831 (2018).
5. P. J. Ko, S. J. Dixon, Protein palmitoylation and cancer. *EMBO Rep.* **19**, e46666 (2018).
6. M. H. Wright, W. P. Heal, D. J. Mann, E. W. Tate, Protein myristoylation in health and disease. *J. Chem. Biol.* **3**, 19–35 (2010).
7. E. Cho, M. Park, Palmitoylation in Alzheimer's disease and other neurodegenerative diseases. *Pharmacol. Res.* **111**, 133–151 (2016).
8. Z. Pei, Y. Xiao, J. Meng, A. Hudmon, T. R. Cummins, Cardiac sodium channel palmitoylation regulates channel availability and myocyte excitability with implications for arrhythmia generation. *Nat. Commun.* **7**, 12035 (2016).
9. M. Hackett, L. Guo, J. Shabanowitz, D. F. Hunt, E. L. Hewlett, Internal lysine palmitoylation in adenylate cyclase toxin from Bordetella pertussis. *Science* **266**, 433–435 (1994).
10. B. Wang *et al.*, Protein N-myristoylation: Functions and mechanisms in control of innate immunity. *Cell. Mol. Immunol.* **18**, 878–888 (2021).
11. J. Sobocinska, P. Roszczenko-Jasinska, A. Ciesielska, K. Kwiatkowska, Protein palmitoylation and its role in bacterial and viral infections. *Front. Immunol.* **8**, 2003 (2017).
12. R. Takada *et al.*, Monounsaturated fatty acid modification of Wnt protein: Its role in Wnt secretion. *Dev. Cell* **11**, 791–801 (2006).
13. F. Galbiati, F. Guzzi, A. I. Magee, G. Milligan, M. Parenti, N-terminal fatty acylation of the alpha-subunit of the G-protein Gi1: Only the myristoylated protein is a substrate for palmitoylation. *Biochem J* **303**, 697–700 (1994).
14. K. Brett *et al.*, Site-specific S-acylation of influenza virus hemagglutinin: The location of the acylation site relative to the membrane border is the decisive factor for attachment of stearate. *J. Biol. Chem.* **289**, 34978–34989 (2014).
15. E. Soupene *et al.*, Association of NMT2 with the acyl-CoA carrier ACBD6 protects the N-myristoyltransferase reaction from palmitoyl-CoA. *J. Lipid Res.* **57**, 288–298 (2016).
16. J. Schulte-Zweckel *et al.*, A hydroxylamine probe for profiling S-acylated fatty acids on proteins. *Chem. Commun.* **55**, 11183–11186 (2019).
17. L. Muszbek, G. Haramura, J. E. Cluette-Brown, E. M. Van Cott, M. Laposata, The pool of fatty acids covalently bound to platelet proteins by thioester linkages can be altered by exogenously supplied fatty acids. *Lipids* **34**, S331–S337 (1999).
18. G. Komaniecki, H. N. Lin, Lysine fatty acylation: Regulatory enzymes, research tools, and biological function. *Front. Cell Dev. Biol.* **9**, 717503 (2021).
19. A. H. Nile, R. N. Hannoush, Fatty acylation of Wnt proteins. *Nat. Chem. Biol.* **12**, 60–69 (2016).
20. A. N. Ken Sato, Miyuki Sato, B. D. Grant, *C. elegans as a Model for Membrane Traffic* (WormBook, Pasadena, CA, 2005–2018).
21. J. L. Watts, M. Ristow, Lipid and carbohydrate metabolism in Caenorhabditis elegans. *Genetics* **207**, 413–446 (2017).
22. M. J. Edmonds, A. Morgan, A systematic analysis of protein palmitoylation in Caenorhabditis elegans. *BMC Genomics* **15**, 841 (2014).
23. Y. Yu *et al.*, An untargeted approach for revealing electrophilic metabolites. *ACS Chem. Biol.* **15**, 3030–3037 (2020).
24. J. J. Galligan *et al.*, Quantitative analysis and discovery of lysine and arginine modifications. *Anal. Chem.* **89**, 1299–1306 (2017).
25. T. Baldensperger, S. D. Sanzo, A. Ori, M. A. Glomb, Quantitation of reactive Acyl-CoA species mediated protein acylation by HPLC-MS/MS. *Anal. Chem.* **91**, 12336–12343 (2019).
26. B. Zhang *et al.*, Acylspermidines are conserved mitochondrial sirtuin-dependent metabolites. *Nat. Chem. Biol.* (2024). https://doi.org/10.1038/s41589-023-01511-2.

27. I. R. Kelsall, J. Zhang, A. Knebel, J. S. C. Arthur, P. Cohen, The E3 ligase HOIL-1 catalyses ester bond formation between ubiquitin and components of the Myddosome in mammalian cells. *Proc. Natl. Acad. Sci. U.S.A.* **116**, 13293–13298 (2019).
28. M. J. Helf, B. W. Fox, A. B. Artyukhin, Y. K. Zhang, F. C. Schroeder, Comparative metabolomics with Metaboseek reveals functions of a conserved fat metabolism pathway in C. elegans. *Nat. Commun.* **13**, 782 (2022).
29. M. Kniazeva, Q. T. Crawford, M. Seiber, C.-Y. Wang, M. Han, Monomethyl branched-chain fatty acids play an essential role in Caenorhabditis elegans development. *PLoS Biol.* **2**, e257 (2004).
30. P. Henry *et al.*, Fatty acids composition of Caenorhabditis elegans using accurate mass GCMS-QTOF. *J. Environ. Sci. Health. B* **51**, 546–552 (2016).
31. M. Zhu *et al.*, Monomethyl branched-chain fatty acid mediates amino acid sensing upstream of mTORC1. *Dev. Cell* **56**, 3171 (2021).
32. T. Meinnel, C. Dian, C. Giglione, Myristoylation, an ancient protein modification mirroring eukaryogenesis and evolution. *Trends Biochem. Sci.* **45**, 619–632 (2020).
33. C. Giglione, T. Meinnel, Mapping the myristoylome through a complete understanding of protein myristoylation biochemistry. *Prog. Lipid Res.* **85**, 101139 (2022).
34. W. W. Kallemeijn *et al.*, Proteome-wide analysis of protein lipidation using chemical probes: In-gel fluorescence visualization, identification and quantification of N-myristoylation, N- and S-acylation, O-cholesterylation, S-farnesylation and S-geranylgeranylation. *Nat. Protoc.* **16**, 5083–5122 (2021).
35. T. Muller, D. Coowar, M. Hanbali, P. Heuschling, B. Luu, Improved synthesis of tocopherol fatty alcohols and analogs: Microglial activation modulators. *Tetrahedron* **62**, 12025–12040 (2006).
36. F. Ye *et al.*, C(sp)–C(sp3) bond formation through Cu-catalyzed cross-coupling of N-Tosylhydrazones and trialkylsilylethynes. *J. Am. Chem. Soc.* **134**, 5742–5745 (2012).
37. B. R. Martin, B. F. Cravatt, Large-scale profiling of protein palmitoylation in mammalian cells. *Nat. Methods* **6**, 135–138 (2009).
38. B. R. Martin, C. Wang, A. Adibekian, S. E. Tully, B. F. Cravatt, Global profiling of dynamic protein palmitoylation. *Nat. Methods* **9**, 84–89 (2012).
39. E. Thinon, J. P. Fernandez, H. Molina, H. C. Hang, Selective enrichment and direct analysis of protein S-Palmitoylation sites. *J. Proteome Res.* **17**, 1907–1922 (2018).
40. I. T. Foe *et al.*, Global analysis of palmitoylated proteins in Toxoplasma gondii. *Cell Host Microbe* **18**, 501–511 (2015).
41. J. Sobocinska *et al.*, Lipopolysaccharide upregulates palmitoylated enzymes of the phosphatidylinositol cycle: An insight from proteomic studies. *Mol. Cell. Proteomics* **17**, 233–254 (2018).
42. M. Blanc, F. P. A. David, F. G. van der Goot, SwissPalm 2: Protein S-Palmitoylation database. *Methods Mol. Biol.* **2009**, 203–214 (2019).
43. C. D'souza-Schorey, P. D. Stahl, Myristoylation is required for the intracellular-localization and endocytic function of Arf6. *Exp. Cell Res.* **221**, 153–159 (1995).
44. Y. Liu, R. A. Kahn, J. H. Prestegard, Structure and membrane interaction of myristoylated ARF1. *Structure* **17**, 79–87 (2009).
45. F. A. Barr, M. Puype, J. Vandekerckhove, G. Warren, GRASP65, a protein involved in the stacking of Golgi cisternae. *Cell* **91**, 253–262 (1997).
46. A. Kuo, C. L. Zhong, W. S. Lane, R. Derynck, Transmembrane transforming growth factor-alpha tethers to the PDZ domain-containing, Golgi membrane-associated protein p59/GRASP55. *EMBO J.* **19**, 6427–6439 (2000).
47. J. Cao *et al.*, HDAC11 regulates type I interferon signaling through defatty-acylation of SHMT2. *Proc. Natl. Acad. Sci. U.S.A.* **116**, 5487–5492 (2019).
48. P. J. Woida, K. J. F. Satchell, The Vibrio cholerae MARTX toxin silences the inflammatory response to cytoskeletal damage before inducing actin cytoskeleton collapse. *Sci. Signal* **13**, eaaw9447 (2020).
49. Y. Zhou *et al.*, N-epsilon-fatty acylation of Rho GTPases by a MARTX toxin effector. *Science* **358**, 528–530 (2017).
50. T. Kosciuk *et al.*, NMT1 and NMT2 are lysine myristoyltransferases regulating the ARF6 GTPase cycle. *Nat. Commun.* **11**, 1067 (2020).
51. G. Hadwiger, S. Dour, S. Arur, P. Fox, M. L. Nonet, A monoclonal antibody toolkit for C. elegans. *PLoS One* **5**, e10161 (2010).
52. W. Ning *et al.*, GPS-Palm: A deep learning-based graphic presentation system for the prediction of S-palmitoylation sites in proteins. *Brief. Bioinform.* **22**, 1836–1847 (2021).
53. P. Gozdzik, F. Magkos, T. Sledzinski, A. Mika, Monomethyl branched-chain fatty acids: Health effects and biological mechanisms. *Prog. Lipid Res.* **90**, 101226 (2023).
54. A. J. Pradhan *et al.*, Protein acylation by saturated very long chain fatty acids and endocytosis are involved in necroptosis. *Cell Chem. Biol.* **28**, 1298–1309.e7 (2021).
55. M. D. Resh, Fatty acylation of proteins: The long and the short of it. *Prog. Lipid Res.* **63**, 120–131 (2016).
56. D. Senyilmaz *et al.*, Regulation of mitochondrial morphology and function by stearoylation of TFR1. *Nature* **525**, 124–128 (2015).
57. B. Chen *et al.*, Auto-fatty acylation of transcription factor RFX3 regulates ciliogenesis. *Proc. Natl. Acad. Sci. U.S.A.* **115**, E8403–E8412 (2018).
58. H. Zhu, H. Shen, A. K. Sewell, M. Kniazeva, M. Han, A novel sphingolipid-TORC1 pathway critically promotes postembryonic development in Caenorhabditis elegans. *Elife* **2**, e00429 (2013).
59. R. Wang, M. Kniazeva, M. Han, Peroxisome protein transportation affects metabolism of branched-chain fatty acids that critically impact growth and development of C. elegans. *PLoS One* **8**, e76270 (2013).
60. J. J. Zhang *et al.*, mmBCFA C17iso ensures endoplasmic reticulum integrity for lipid droplet growth. *J. Cell Biol.* **220**, e202102122 (2021).
61. J. S. Hoki *et al.*, Deep interrogation of metabolism using a pathway-targeted click-chemistry approach. *J. Am. Chem. Soc.* **142**, 18449–18459 (2020).
62. R. S. Bhatnagar *et al.*, Titration calorimetric analysis of AcylCoA recognition by myristoylCoA:protein N-myristoyltransferase. *Biochemistry* **36**, 6700–6708 (1997).
63. M. S. Rana *et al.*, Fatty acyl recognition and transfer by an integral membrane S-acyltransferase. *Science* **359**, eaao6326 (2018).
64. C. Dian *et al.*, High-resolution snapshots of human N-myristoyltransferase in action illuminate a mechanism promoting N-terminal Lys and Gly myristoylation. *Nat. Commun.* **11**, 1132 (2020).
65. X. Liang *et al.*, Heterogeneous fatty acylation of Src family kinases with polyunsaturated fatty acids regulates raft localization and signal transduction. *J. Biol. Chem.* **276**, 30987–30994 (2001).
66. S. L. Bursten, R. M. Locksley, J. L. Ryan, D. H. Lovett, Acylation of monocyte and glomerular mesangial cell proteins. Myristyl acylation of the interleukin 1 precursors. *J. Clin. Invest.* **82**, 1479–1488 (1988).
67. Y. V. Karpievitch, A. R. Dabney, R. D. Smith, Normalization and missing value imputation for label-free LC-MS analysis. *BMC Bioinf.* **13**, S5 (2012).
68. S. X. Ge, D. M. Jung, R. A. Yao, ShinyGO: A graphical gene-set enrichment tool for animals and plants. *Bioinformatics* **36**, 2628–2629 (2020).
69. B. Zhang *et al.*, Amino acid- and protein-specificity of protein fatty acylation in C. elegans. Mass Spectrometry Interactive Virtual Environment. https://massive.ucsd.edu/ProteoSAFe/dataset.jsp?task=d92e8fac06d24be793ffdccdc1ed7120. Deposited 8 November 2023.